Cavitation at triple nodes in α-zirconium polycrystals

Sabine Caré, André Zaoui

CAVITATION AT TRIPLE NODES IN α-ZIRCONIUM POLYCRYSTALS

S. CARÉ and A. ZAOUI

Laboratoire de Mécanique des Solides, CNRS URA 317, Ecole Polytechnique, F 91128 Palaiseau Cédex, France

Abstract—The damage mechanisms of α-zirconium polycrystals in tension at room temperature and their dependence on texture and grain size are investigated. Ductile damage proceeds by growth of cavities appearing at triple nodes; at larger strain, other cavities nucleate at precipitate platelets. The cavitation kinetics depend on the tension direction; they are lower the coarser the grains. For a better understanding of the cavity formation at triple nodes, the internal stress field due to intergranular plastic incompatibility is estimated. The mean stress exhibits a logarithmic singularity on the triple junction. By combining this property with some experimentally determined features of the cavity growth (tubular shape along the **c** axis and growth by activation of prismatic glide), a crystallographic orientation-dependent cavitation criterion is derived. The determination of the grains orientation by the E.B.S.D. technique leads to a satisfactory comparison of the model predictions with the observations.

Résumé—On analyse les mécanismes d'endommagement du zirconium α polycristallin en traction simple à température ambiante et leur sensibilité à la texture et à la taille de grain. L'endommagement ductile commence par une croissance de cavités aux jonctions triples; d'autres cavités se forment ultérieurement sur des plaquettes de précipités. La cinétique de cavitation dépend de la direction de sollicitation; elle diminue pour les tailles de grains élevées. Pour expliquer la formation des cavités aux joints triples, on évalue le champ de contraintes internes associées aux incompatibilités plastiques intergranulaires. La contrainte moyenne présente une singularité logarithmique sur l'arête triple. En associant à cette propriété certains aspects expérimentaux de la croissance des cavités (forme tubulaire selon l'axe **c**, croissance par glissements prismatiques), on élabore un critère de cavitation sensible à l'orientation cristallographique. La détermination de l'orientation des grains par E.B.S.D. permet une confrontation satisfaisante des prévisions du modèle aux observations.

1. INTRODUCTION

Zirconium and zirconium alloys are commonly used for structural components and fuel cladding in nuclear power reactors for their very low thermal neutron capture cross-section, as well as for tanks used in the reprocessing of fuel elements, because of their high chemical resistance to nitric acid between 300 and 500 K. In both cases, a good knowledge of their mechanical behaviour is needed too in order to improve the forming processes and the prediction of the structures lifetime; so, damage mechanisms have to be identified and their dependency on metallurgical and mechanical material parameters must be well known.

Paradoxically, rather a small amount of work has been done up to now in view of the identification of the damage mechanisms of zirconium. Published results indicate only that fracture at room temperature and above is of the ductile type; tensile tests show that it follows necking and that the fracture surface has a dimpled appearance. Nevertheless, damage nucleation may be analysed by referring to results obtained on titanium, which presents some similarities with α-zirconium, due to a similar electronic structure [1]: especially, from a study on a commercially produced titanium, Donoso *et al.* [2] suggest that voids nucleate at grain boundary triple points or at grain boundaries, but they do not give an interpretation of this phenomenon and the possible role of precipitates or inclusions on such a void nucleation on the grain boundaries remains an open question.

The aim of this study is to get a better understanding of the damage behaviour of α-zirconium polycrystals at room temperature, excluding final failure analysis. Keeping in mind the use of zirconium rolled sheets for fuel reprocessing tanks, we investigate the influence of the crystallographic texture on ductile cavitation and the role of precipitates in this process. In addition, since materials with coarsened grains have been used for an easier identification of the damage mechanisms, the influence of grain size has been checked too. Finally, a model taking these effects into account is proposed and compared to experimental evidences based on micrographic observations and use of the E.B.S.D. (Electron Back-Scattering Diffraction) technique.

Table 1. Chemical analysis of the zirconium samples (by wt)

Zr + Hf	>99.2%	C	56 ppm
Ni	60 ppm	H	3 ppm
Fe + Cr	776 ppm	N	24 ppm
Sn	1240 ppm	O	1250 ppm

2. EXPERIMENTAL PROCEDURE

The material under investigation is a commercial α-zirconium product (coded as Zr-702), received as cold-rolled 8 mm thick sheets. The chemical analysis is given in Table 1. The average grain size of the as-received material is about 15 μm (measured as a mean linear intercept). In addition, part of the studied material has been thermomechanically treated (3% strain followed by 5 h heating at 710°C), in order to coarsen the grains up to about 100 μm.

At room temperature, zirconium exhibits a hexagonal close-packed crystal structure, with a c/a ratio of 1.593 (i.e. a slight compression in the $\langle 0001 \rangle$ **c** direction, compared to the ideal ratio of 1.633). At 865°C, zirconium undergoes an allotropic transformation from the low temperature H.C.P. α phase to the B.C.C. β phase. The crystallographic texture of the as-received specimens is given in Fig. 1. The **c** axes are preferentially perpendicular to the rolling direction (R.D.) with a tendency to spread by 40° towards the transverse direction (T.D.). The material with coarser grains exhibits the same texture.

Surfaces suitable for metallographic analysis are prepared by grinding through 1200 grit papers, followed by an electrolytic polishing with perchloric (20%) and acetic acids (80%), held at 10°C under 24 V, to reveal grain boundaries; then a chemical polishing is performed for revealing precipitates (with a solution of 12% nitric, 65% glycerol and 23% fluorhydric acids). These techniques allow the observation of precipitates of a micronic size. Most of them form platelets parallel to the rolling plane, distributed randomly with respect to the grain boundaries. The

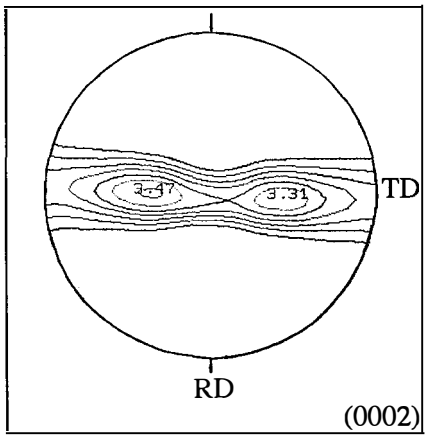

Fig. 1. Texture of the used Zr sheet (CEREM/SRMA Document).

Table 2. Tensile properties of the zirconium samples

	(R.D.): Small/coarse grained material	(T.D.): Small/coarse grained material
Yield stress	290/200 MPa	360/290 MPa
Ultimate tensile stress	430/400 MPa	430/400 MPa
Strain to necking	16/16%	11/11%

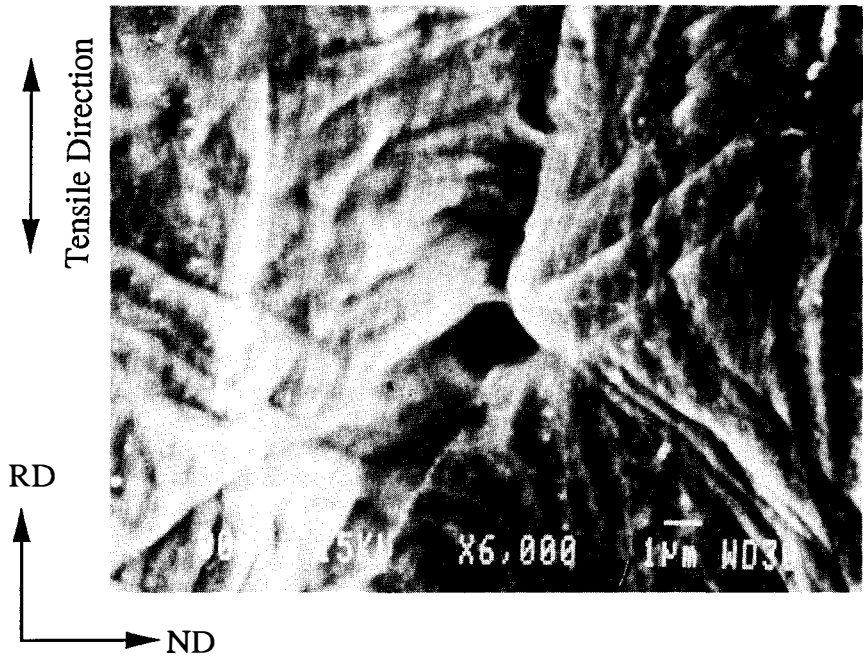

Fig. 2. Cavity at a triple node in the small grained material deformed along the rolling direction (the specimen has been chemically polished).

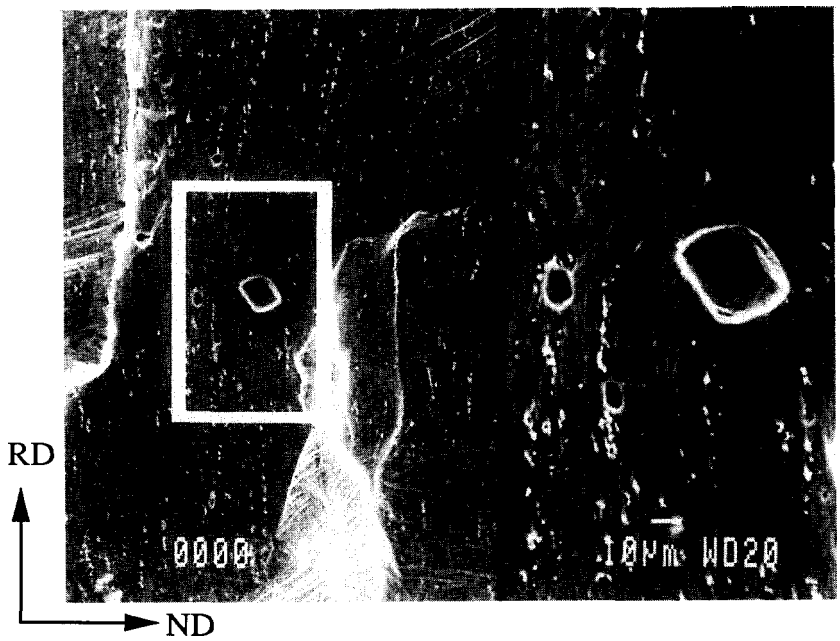

Fig. 3. Cavity at a precipitate platelets in the coarse grained material deformed along the rolling direction (the specimen has been chemically polished).

E.D.S. technique reveals iron, nickel and chromium, according to the general formulae $Zr_2(Ni, Fe)$ and $Zr(Cr, Fe)_2$ [3]. Due to the low solubility of these addition elements, the precipitation state is not modified by the heat treatment used for the grain coarsening.

Tensile tests are performed at room temperature on an Instron machine at $2.8 \times 10^{-4}\,s^{-1}$ strain rate along (R.D.) and (T.D.). The mechanical characteristics are given in Table 2. For different strain levels, the tested samples are cut parallel to their axis, prepared as depicted hereabove and examined under a Scanning Electron Microscope (S.E.M.). Additional tensile tests are performed inside the S.E.M. along the two reference directions.

Square fiducial microgrids with a $5\,\mu m$ pitch deposited on the sample surface allow to follow the evolution of the strain inhomogeneities and the inception and evolution of damage. The microgrids are made of gold by means of a microelectrolithographic technique [4].

Table 3. Probability of location of the cavities at triple nodes and elsewhere for three strain levels (in each case, probability for precipitates to be present near the cavity) for a small grained material pulled along (R.D.) up to fracture

	Location of cavities	
	Triple nodes	Intragranular cavities
ϵ_A	66% (45% at precipitate platelets)	34% (81% at precipitate platelets)
$\epsilon_B (>\epsilon_A)$	56% (56%)	44% (78%)
$\epsilon_C (>\epsilon_B)$	49% (46%)	51% (75%)

3. EXPERIMENTAL RESULTS

3.1. Void initiation

In both the small and coarse grained materials, the first damaging events which can be seen by S.E.M. are subsequent to the inception of necking. S.E.M. observations on sectioned samples or performed during *in situ* tensile tests show that, whatever the tensile test direction, voids nucleate first at grain boundary triple points or at grain boundary irregularities throughout the samples. Figure 2 shows such a cavity nucleated at a grain boundary triple node.

A second population of cavities appears at precipitate platelets at higher strain levels (Fig. 3). The densities of these two families can be compared by analysing their distribution on a sample pulled up to fracture as a function of the distance to the fracture surface. Since the local strain decreases with this distance, such a measurement can give information on the strain dependence of the density of cavities. The ratio of the density of cavities located at precipitate platelets to the density of those located at grain boundary triple points is found to increase as the distance to the fracture surface decreases, i.e. to increase with strain (Table 3). Table 4 shows that, at the commencement of cavitation, the probability that

Table 4. Influence of the strain level on the damage mechanisms. The sample is deformed by 24% along the rolling direction

Void initiation	With precipitates	Without precipitates
At triple nodes: 75%	84%	16%
Intragranular cavities: 25%	87%	13%

a cavity appears at a grain boundary triple node is larger when this node is associated with a precipitate platelet. Nevertheless it has been checked that cavities may nucleate at grain boundary triple points even when no precipitate is observed by S.E.M. in the vicinity of the junction.

When tensile tests are performed along the transverse direction, twins are activated; they can induce the nucleation of cavities because of the stress concentration at their tips [5]; nevertheless, few such cavities are observed at twin tips.

3.2. Void growth

Cavities are always growing on one side of a grain boundary into only one grain. This growth is limited by the grain size or by the coalescence of cavities; it is responsible for the development of large smooth dimples on the fracture surface. Cavity growth mechanisms may be identified from the observations of the fracture surface.

In the coarse grained material, dimples are tubular with an average width of 10 μm and a length of about

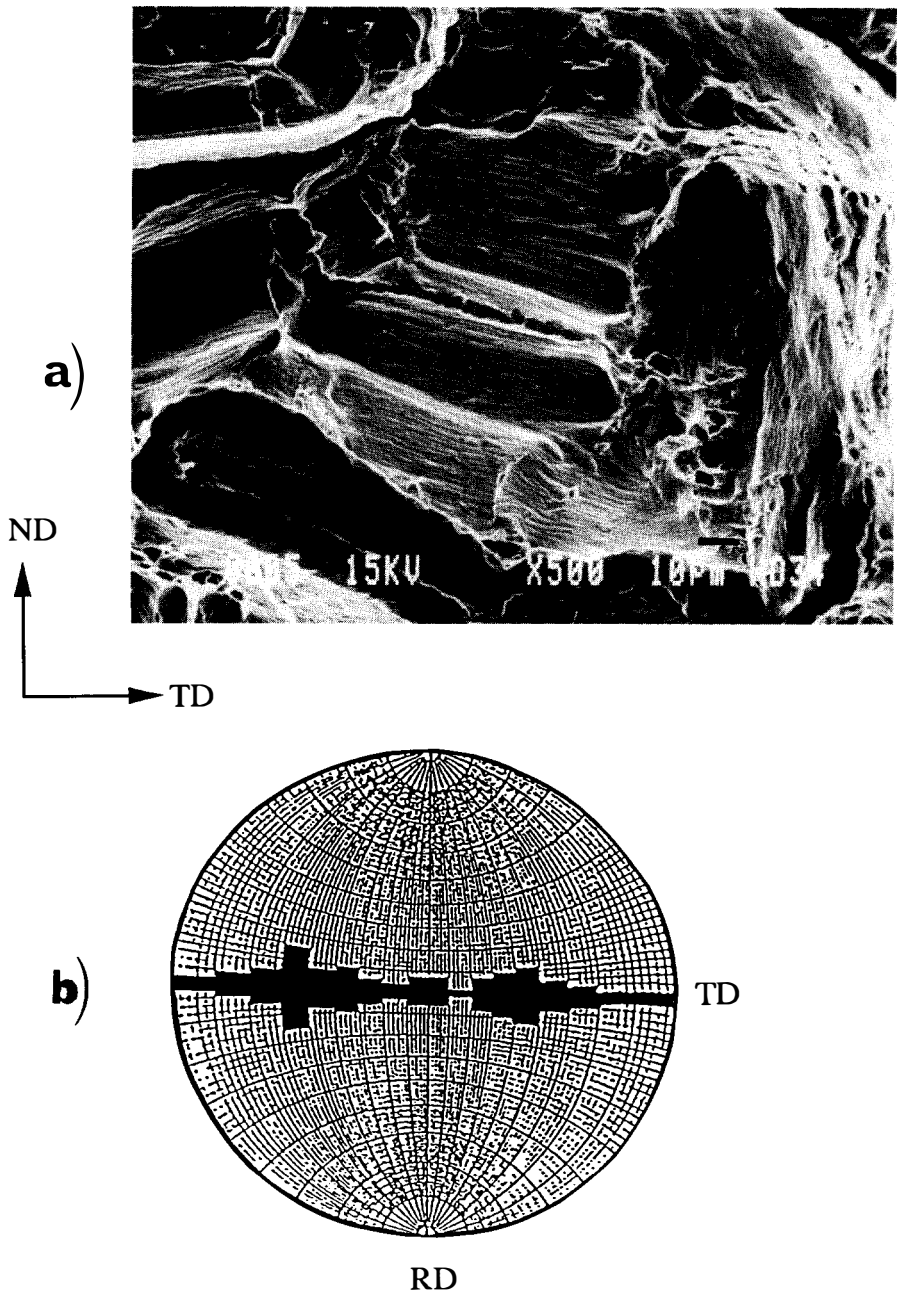

Fig. 4. (a) Fracture surface of the coarse grained material deformed along the rolling direction. (b) Orientation frequencies of the tubular dimples supposed to lie along the **c** axis.

Fig. 5. Coarse grained material deformed along the transverse direction. In plane A, a circular section of a cavity is observed; in plane B, the same cavity looks tubular.

100 μm. Several cavities may appear and grow in one grain, leading to several tubular dimples. On the fracture surface of a sample pulled along the rolling direction, the angles between the tubular axes and the transverse direction have been measured (the axes are supposed to lie in a plane orthogonal to the rolling direction) and plotted on a stereographic projection (Fig. 4). It can be noticed that the resulting "pole figure" is quite similar to the one which refers to the crystallographic texture (see Fig. 1). Note that the texture remains unchanged during such a test [6]. This comparison confirms the fact that the tubular dimples are elongated along the **c** direction.

When tensile tests are performed along the transverse direction, tubular axes are observed to be nearly perpendicular to the rolling direction; so are the **c** axes. On Fig. 5, one can see two cross-sections of one cavity by two perpendicular planes: in plane A (TD, RD), the cross-section is almost circular whereas in plane B (TD, ND), the cavity looks tubular. It is roughly perpendicular to the tensile direction (TD), which is a situation favourable for growth by plastic glide on prismatic planes.

Such a growth of the cavities along a **c** direction suggests that it involves prismatic slip. By use of the E.B.S.D. technique, the crystallographic orientation of grains where a cavity is growing can be determined. When the **c** axis is parallel to the observation plane, cavities are long and tubular. When it is perpendicular to the observation plane, they have a rounded shape and prismatic slip bands can be observed in the vicinity; most of the time, two active slip systems can be observed in the grain where a cavity is growing. In a sample with large grains, Watson *et al.* [7] have observed hexagonal cavities involving three slip bands. By using

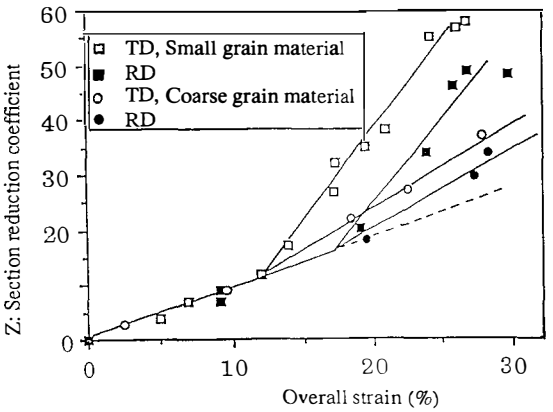

Fig. 6. The section area reduction coefficient versus the overall strain for both the (R.D.) and (T.D.) tensile axes directions (small and coarse grained materials).

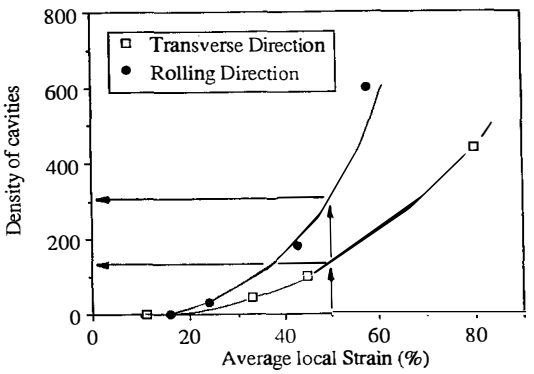

Fig. 7. Influence of the strain level in the necking region on the cavity density. Cavities are counted whatever their size, at magnification 200× (small grained material).

the E.B.S.D. technique on a β-treated zirconium, Crépin and Bretheau [8] have proved that the activation of several sets of two prismatic slip systems is responsible for the growth of hexagonal cavities.

In small grained samples, dimples are no more tubular but roughly equiaxed. Growth mechanisms are supposed to be the same but, in this case, the cavity growth is limited by the grain size (about 15 μm).

As straining goes on, the coalescence process leads to the formation of ligaments. The general correspondence between the size of the grains and that of the cuplets observed on the fracture surface indicates that only one void is nucleated per grain on average, as a result of the extensive local deformation preceding fracture. Through further deformation, the void growth is accompanied by an important stretching of the ligaments between the voids: the ligaments consist of material originating from the region near the grain boundaries. When more than one void per grain is nucleated (in the material with coarse grains), the cuplets are tubular and only part of the wall of each cuplet exists in the intergranular material.

3.3. Influence of the tensile test direction on cavitation

In view of a quantitative analysis of the influence of the tensile test direction on the cavitation kinetics, longitudinal sections through the strained region of tensile specimens have been cut and investigated. Cavities are counted without reference to their size. Since our experimental procedures don't allow one to distinguish nucleation and growth of cavities unambiguously, we refer to cavitation as the cavity "formation", which includes both their nucleation and part of their growth. Cavities are mainly present in the necked region of the tensile specimens where the strain level is larger.

In order to evaluate this effect quantitatively, it is first necessary to measure the cross-section area reduction in the necking region. On Fig. 6, the section reduction coefficient Z defined by $Z = (S_0 - S)/S_0$ (where S_0 is the initial area and S the area after necking) is plotted as a function of the overall strain, for the small and coarse grained materials and for the two (T.D.) and (R.D.) tensile directions. At a 10% strain level in the first case and 16% in the second case, the slope changes drastically. In both cases, this slope change can be interpreted as denoting the inception of necking. Since the cavities appear in the necked area, the density of cavities has to be plotted versus the average local strain ϵ_n in this area instead of the overall one. The strain ϵ_n can be determined from Fig. 6, through the relation:

$$\epsilon_n = \ln(S_0/S) = -\ln(1 - Z). \qquad (1)$$

It can reach 60%, which is in good agreement with the local strain as measured by the microgrids technique over a representative volume element. Figure 7 shows that, after the inception of necking, the density of cavities is sharply increasing with ϵ_n. This variation is strongly dependent on the tensile test direction: at a given strain ϵ_n the density of cavities is about 60% lower when the tensile direction lies along (T.D.) than when it lies along (R.D.).

3.4. Influence of the grain size

The above quantitative analysis has been performed only on the material with small grains. Nevertheless, some specimens with coarser grains deformed up to fracture have been sectioned longitudinally and observed too. Two qualitative conclusions may be drawn from these observations: first, as for the small grained material, the density of cavities is much lower when the tensile tests are performed along (T.D.) than along (R.D.); secondly, as a whole, the density of cavities is smaller than in the small grained material. Such a grain size effect has been reported by Forsher [9] too on a similar material, α-annealed at 840°C for 48 h. This heat treatment resulted in a banded structure consisting of both small and coarse grains. The tensile tested specimen showed a predominance of cavities in the small grained region. Nevertheless Forsher didn't give any explanation of this effect.

3.5. Conclusion

The tensile test direction and the grain size have a strong influence on the cavitation kinetics. The formation of the cavities is clearly dependent on the stress triaxiality and on the presence of precipitates. However, none of these factors can explain the influence of the tensile test direction of the cavitation kinetics since they are not orientation-dependent. The voids nucleate first at grain boundaries triple points; they develop along the **c** direction through the plastic activity of two prismatic slip systems at least.

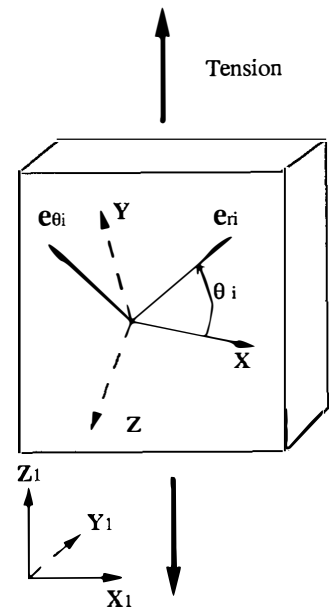

Fig. 8. Definition of different axes systems (**X**, **Y**, **Z**), ($\mathbf{X}_1$, $\mathbf{Y}_1$, $\mathbf{Z}_1$) and ($\mathbf{e}_r$, $\mathbf{e}_\theta$, **Z**).

Damage mechanisms at grain boundaries and near triple nodes have been the matter of intensive study for a long time, but such studies have been mainly concerned with the role of precipitates [10, 11], the development of microcracking [12], the formation of "wedge" or "round" cracks during creep [13] or with grain boundary sliding [14]. To the best of our knowledge, no interpretation has been proposed up to now for the formation of rounded (cylindrical) cavities at triple nodes in ductile polycrystals under monotonic loading at room temperature. In the following, special attention will be paid to this point by taking the observed characteristics of the growth mode of cavities into account in order to interpret the influence of the tensile test direction on the cavitation kinetics. It is soon worth noticing that when a tensile

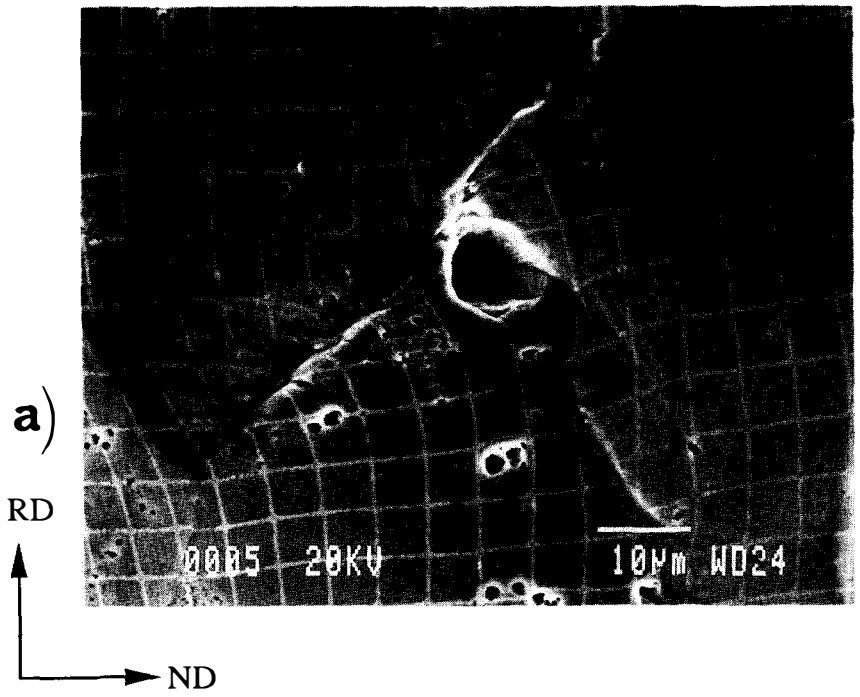

Grain I: Mk=0.19; **0.44**; 0.25
Grain II: Mk=0.18; **0.49; 0.32**
Grain III: Mk=0.22; **0.50; 0.28**

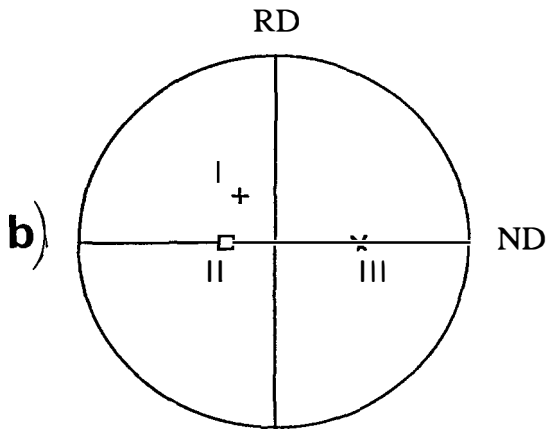

Fig. 9. (a) Cavity present at a triple node. The tensile test is performed along the rolling direction (ϵ = 20%). Microgrids show that grains I and II are more deformed than grain III. (b) Schmid factors for the prismatic slip systems in each grain and [0002] pole figure for grains I, II and III.

test is performed along the rolling direction, the **c** axes are preferentially perpendicular to (R.D.), whereas they spread by 40° towards the tensile test direction when it is performed along (T.D.): so, the crystallographic texture is likely to play a role in the sensitivity of cavitation to the tensile test direction.

4. INTERNAL STRESSES AT TRIPLE NODES AND CAVITATION

Since cavities nucleate first at grain boundary triple points even when precipitates are not present here, it may be thought that this phenomenon is ruled by internal stress concentrations associated with plastic incompatibility which may exist around these points. In order to get a quantitative estimate of this effect, calculations of the internal stress field developing in tricrystals could be used [15, 16, 12]: they are concerned with infinite plane boundaries and uniformly plastically deformed grains, according to an elastic accommodation scheme, and they show that a logarithmic stress singularity occurs at the multiple node (not that, according to Belov [17], various other anomalies could occur near wedge-like inhomogeneities . . .). In the following, these analytical calculations will be applied to the situations depicted above in order to be compared with experimental evidence of void formation at specific triple nodes; additional assumptions deriving from the observed cavity growth mechanisms will be taken into account in order to propose a cavitation criterion which would be in agreement with the main conclusions of the experimental analysis.

4.1. *Internal stresses in an infinite multicrystal*

The main results of the analysis of the internal stress field in an infinite multicrystal may be summed up as follows. The considered body exhibits three (or more, n say) grain boundaries which are concurrent along **OZ**. Each plane grain boundary (i), with the angle θ_i from **OX** and the unit outward normal vector $\mathbf{e}_\theta^i$ (Fig. 8), separates grains (i) and $(i+1)$. Using cylindric coordinates (r, θ, z), the plastic strain field can be written anywhere as follows:

$$\epsilon^p(\theta) = \epsilon_1^p + \sum_{k=1}^{n} (\epsilon_{k+1}^p - \epsilon_k^p) Y(\theta - \theta_k) \qquad 0 < \theta \leqslant 2\pi \quad (2)$$

where ϵ_k^p is constant for any $k \in [1, n]$ and $Y(x)$ is the unit step function. Thus, any grain (i) undergoes a uniform plastic strain ϵ_i^p. Elasticity is assumed to be uniform and isotropic with μ the shear modulus and ν the Poisson ratio. (Note that Fisher and Renken [18] indicate that the elastic behaviour of zirconium is nearly isotropic.) The resulting internal stress field is calculated according to an elastic accommodation assumption: it is derived by superposition of the stress field contributions associated with each grain boundary (i). The main part (i.e. far from the outer surface of the body) of such a contribution reads as follows:

$$\begin{aligned}
\sigma_{rr}^{(i)} &= -\frac{\mu}{2\pi(1-\nu)}\left[(b_{rr}^{(i)} + \nu b_{zz}^{(i)})\left(2\delta_i \cos^2\phi_i - \sin 2\phi_i \ln\frac{r}{R^{(i)}}\right) - \cdots \right. \\
&\quad \left. \cdots - (b_{rr}^{(i)} + b_{zz}^{(i)}) \sin\phi_i \cos\phi_i + b_{\theta r}^{(i)}\left(\nu - \ln\frac{r}{R^{(i)}}\right)\right] \\
\sigma_{\theta\theta}^{(i)} &= -\frac{\mu}{2\pi(1-\nu)}\left[(b_{rr}^{(i)} + \nu b_{zz}^{(i)})\left(2\delta_i \sin^2\phi_i + \sin 2\phi_i \ln\frac{r}{R^{(i)}}\right) + \cdots \right. \\
&\quad \left. \cdots + (b_{rr}^{(i)} + b_{zz}^{(i)}) \sin\phi_i \cos\phi_i + b_{\theta r}^{(i)}\left(1 + \nu - \ln\frac{r}{R^{(i)}}\right)\right] \\
\sigma_{zz}^{(i)} &= -\frac{\mu}{2\pi(1-\nu)}\left[2\delta_i (b_{zz}^{(i)} + \nu b_{rr}^{(i)}) - \nu b_{\theta r}^{(i)}\left(2\ln\frac{r}{R^{(i)}} + 1\right)\right] \\
\sigma_{\theta z}^{(i)} &= -\frac{\mu}{\pi} b_{rz}^{(i)}\left[-\delta_i \sin\phi_i - \cos\phi_i\left(\frac{1}{2} - \ln\frac{r}{R^{(i)}}\right)\right] \\
\sigma_{rz}^{(i)} &= -\frac{\mu}{\pi} b_{rz}^{(i)}\left[\delta_i \cos\phi_i - \sin\phi_i\left(\frac{1}{2} + \ln\frac{r}{R^{(i)}}\right)\right] \\
\sigma_{\theta r}^{(i)} &= -\frac{\mu}{2\pi(1-\nu)}\left[(b_{rr}^{(i)} + b_{zz}^{(i)}) \sin^2\phi_i - (b_{rr}^{(i)} + \nu b_{zz}^{(i)})\left(\delta_i \sin 2\phi_i + \cos 2\phi_i \ln\frac{r}{R^{(i)}}\right)\right]
\end{aligned} \quad (3)$$

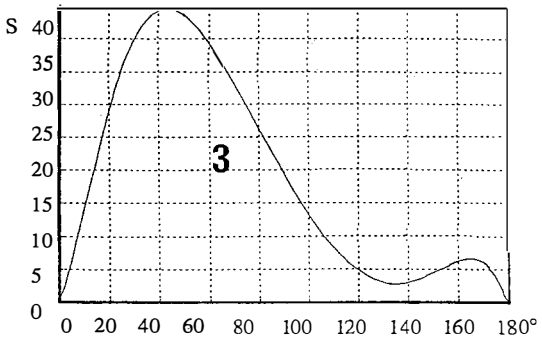

Fig. 10. The junction is assumed to be perpendicular to the tensile test direction, the angle between $\mathbf{X}_1$ and **Z** varies from 0° up to 180°. Case of Fig. 9.

with $\phi_i = \theta - \theta_i$, $\delta_i = \pi \operatorname{sgn} \phi_i - \phi_i$, $R^{(i)}$ a constant of the order of the grain size, which will be the same for all the grains in the following ($R^{(i)} = R \forall i$) and $\mathbf{b}^{(i)} = \epsilon^{\mathrm{p}}_{i+1} - \epsilon^{\mathrm{p}}_{i}$.

These results indicate that the internal stress field exhibits a logarithmic singularity at $r = 0$ which could be responsible for a preferred cavity nucleation at triple nodes. Since, as indicated above, we cannot separate experimentally the nucleation of a cavity from the first stages of its growth, we focus attention on the mean stress $\sigma_{\mathrm{m}} = \frac{1}{3}\mathrm{Tr}(\sigma)$ which is likely to rule the cavity growth. It is singular too and it reads:

$$\sigma_{\mathrm{m}} = -\frac{\mu(1+\nu)}{3\pi(1-\nu)} \sum_{i=1}^{n} \times \left[\delta_i (b^{(i)}_{rr} + \nu b^{(i)}_{zz}) + b^{(i)}_{\theta r} \left(\tfrac{1}{2} - \ln \frac{r}{R} \right) \right]. \quad (4)$$

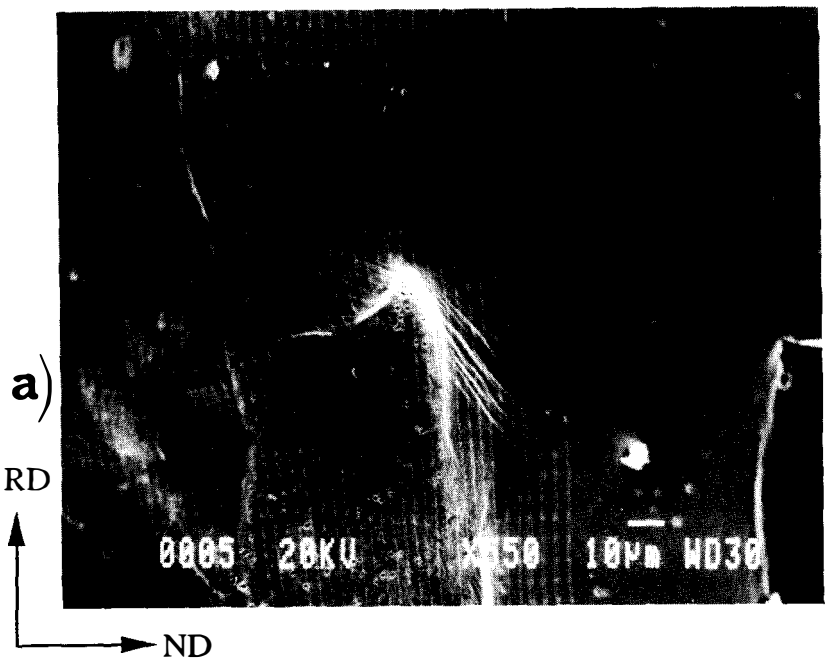

Grain I: Mk=0.13; **0.48**; **0.34**
Grain II: Mk=0.05; **0.41**; **0.45**
Grain III: Mk=0.01; **0.40**; **0.39**

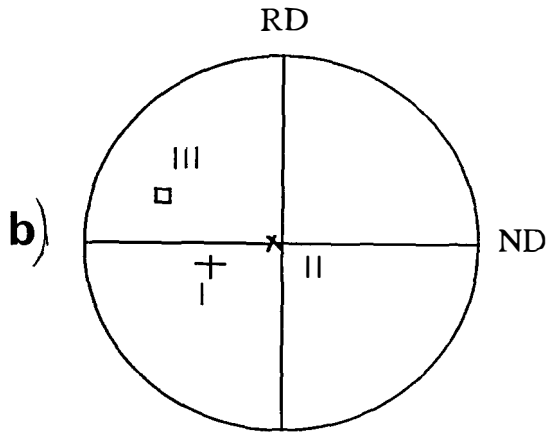

Fig. 11. (a) Grain boundary triple node without a cavity. The tensile test is performed along the rolling direction ($\epsilon = 20\%$). (b) [0002] pole figure for grains I, II and III and Schmid factors for the prismatic slip systems in each grain.

From this expression, we propose to extract the singular term which has the form $k \cdot \ln r$ and to check the sign of k: since $\ln r \to -\infty$ as $r \to 0$, when $k < 0$ the mean stress singularity is positive (and the hydrostatic pressure negative) so that the internal stress field can help the cavity growth whereas when $k > 0$ it opposes cavitation. Note that the sign of k is opposite to the one of s defined by:

$$s = -\sum_{i=1}^{n} b_{\theta r}^{(i)}. \tag{5}$$

So, a tentative criterion would be:

$s > 0$: propitious to cavitation

$s < 0$: not propitious to cavitation. (6)

Nevertheless additional arguments have to be considered in order to elaborate an operative cavitation criterion which could be checked experimentally.

4.2. Application

The derivation of s from experimental measurements would need 3D informations which are out of reach, namely the θ_i angles in order to fix the position of the (i) grain boundaries in the plane **(X, Y)** and the direction **OZ** of the junction. As a matter of fact, this direction cannot be derived from the inspection of the sample surfaces. So we first choose to deal with situations which would be *the most propitious to cavitation*: according to the conclusions of the experimental investigation, we consider that the junction is parallel to the elongation axis of a potential (or actual) tubular cavity growing in a given grain, i.e. parallel to the **c** axis of such a grain. If the lattice orientations of the involved grains (which will be determined by the E.B.S.D. technique) are known, this assumption allows one to identify the geometrical data of the problem completely (see Appendix). In some cases, more general situations will be investigated too (see the following).

The mechanical aspects involve the determination of tensors $\mathbf{b}^{(i)}$ which cannot be obtained from direct measurements anymore. So, additional assumptions must be made. From the above experimental evidences (growth of cavities through the activation of two prismatic slip systems), we conclude that cavitation requires that two prismatic slip systems at least be sufficiently well oriented to be plastically active. In addition, we neglect the internal stress field when estimating this plastic slip ability and consider the applied stress only: practically, this means that we require that two prismatic slip systems have a Schmid factor M large enough (larger than some critical value, M_c say) in order that cavitation may develop. If several grains fulfill this condition, we choose the one with the highest Schmid factors for the potential location of the cavity. Finally, we have to estimate the plastic shear amount on active systems [i.e. γ_k on systems (k) such that $M_k \geqslant M_c$, whatever the grain they belong to]: we assume that it is proportional to the associated Schmid factor $(\gamma_k = M_k \gamma^0)$. Consequently, $\mathbf{b}^{(i)}$ is given by:

$$\mathbf{b}^{(i)} = \gamma^0 (\Sigma_k M_k^{(i+1)} \mathbf{M}_k^{(i+1)} - \Sigma_1 M_1^{(i)} \mathbf{M}_1^{(i)}) \quad \gamma^0 \geqslant 0 \tag{7}$$

where $\mathbf{M}_k^{(i)}$ is the Schmid tensor of system (k) in grain (i) defined by:

$$\mathbf{M}_k^{(i)} = \tfrac{1}{2}(\mathbf{m}_k^{(i)} \otimes \mathbf{n}_k^{(i)} + \mathbf{n}_k^{(i)} \otimes \mathbf{m}_k^{(i)}) \tag{8}$$

with $\mathbf{n}_k$ the unit normal to the slip plane, $\mathbf{m}_k$ the unit vector of the slip direction and $\otimes$ denoting a dyadic product. The (k) and (l) systems involved in equation (7) are such that their Schmid factors M_k defined by $M_k = \mathbf{t} \cdot \mathbf{M}_k \cdot \mathbf{t}$, where $\mathbf{t}$ is the unit vector along the tensile axis, are larger than M_c.

Since we are interested only in the sign and the relative values of s for different situations and we have no means to measure γ^0, our practical cavitation criterion can be ruled by s/γ^0. So we define the new parameter S by:

$$S = -\frac{100}{\gamma^0} \sum_{i=1}^{n} b_{\theta r}^{(i)} \tag{9}$$

and by the associated assumptions described above concerning the orientation of the junction and the slip systems plastic activity. Consequently, M_c is the only fitting parameter. Note that, due to strain-hardening, it has to be considered as a decreasing function of the overall strain (or stress) level.

4.3. Comparison between predictions and observations

The above criterion has been checked in a number (about 30) of experimental situations of junctions with or without a cavity at the triple node for a tensile direction along (R.D.). As a whole, from a statistical point of view, a quite good agreement was found between the predictions and the observations by taking an M_c factor of the order of 0.26. In all the checked cases with a cavity present at the triple node, S was found to be positive. Conversely, when no

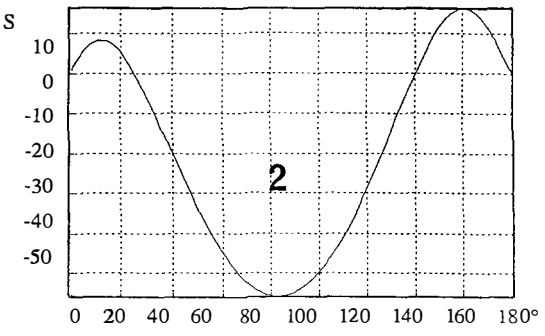

Fig. 12. The junction is assumed to be perpendicular to the tensile test direction, the angle between $\mathbf{X}_1$ and $\mathbf{Z}$ varies from 0° up to 180°. Case of Fig. 11.

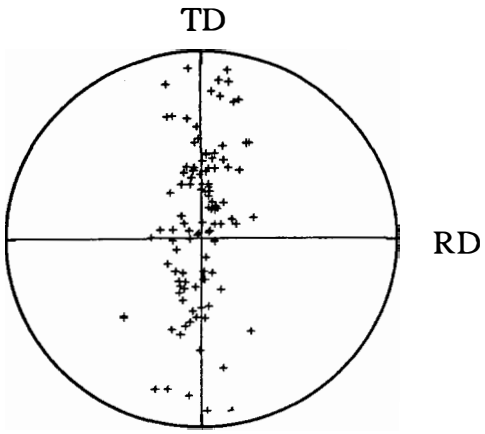

Fig. 13. Measured lattice orientations of 120 grains in a representative area element.

cavity was present, S was found to be negative in most (more than 90%) cases, when assuming that the cavity would grow in the grain with the highest Schmid factors (i.e. assuming the junction to be parallel to the **c** axis of this grain). If we remember that the proposed criterion is rather favourable to cavitation, due to the choice of the direction junction in the calculation, this result can be thought to be quite conclusive. Note that in all the cases, two prismatic systems were considered to be active since their Schmid factor was larger than M_c.

In order to illustrate the analysis procedure and to discuss the influence of the junction orientation on the conclusions, two typical cases are reported now with more details. The first one refers to a situation where a cavity is present at the triple node. First, the crystallographic orientation of each grain is identified by the E.B.S.D. technique, so that all the $\mathbf{M}^k$ tensors can be calculated in each grain. Since the **c** axes are nearly perpendicular to the observed surface (Fig. 9), prismatic slip lines are hardly visible by S.E.M.; but, with the help of the microgrids, grains I and II clearly appear more deformed than grain III far enough (by a few microns) from the junction. The deformed grids would support the assumption of a double slip activity in grains I and II instead of a single slip one in grain III; considering the involved Schmid factors in the three grains, this leads to estimated M_c as 0.26. Since the cavity has grown in grain I, the triple junction is assumed to be parallel to the **c** axis of this grain. The calculation yields $S = +20$. So, the sign of the mean stress singularity is in agreement with the observation. Moreover, the cavity is actually growing in the grain with the highest Schmid factors.

In addition, the dependence of the sign of S on the junction orientation can be checked by considering a continuous variation of this orientation perpendicular to (R.D.): Fig. 10 shows that S remains positive in any case, which enhances the foregoing conclusion.

The second example is concerned with a typical situation without any cavity observable at the triple node. In grains I and II, two prismatic slip lines are visible (Fig. 11), which fits with the calculated Schmid factors. Firstly, we assume that the junction line is parallel to the **c** axis of grain II, which has the largest Schmid factors: the resulting calculated S value is -53, in agreement with the observation (no cavity). This result is then corroborated by the calculation of S for an arbitrary orientation of the junction line in a plane normal to (R.D.): here again (Fig. 12), S is shown to be negative in the main part of the checked angular range.

4.4. Influence of the tensile test direction

A smaller number of such tests have been performed when the tensile axis lies along (T.D.). Nevertheless, similar conclusions were drawn, except that twinning may occur [19, 20] and has then to be taken into account: an example of such a situation will be given in the following. In order to check whether the proposed model could account for the observed influence of the tensile test direction on the cavitation kinetics, we chose an area of a virgin sample with coarse grains, likely to be representative of the microstructure, and we measured up to 120 crystallographic grain orientations by the E.B.S.D. technique (Fig. 13). The S factor was calculated for 30 triple nodes by applying the above defined criterion for both the (R.D.) and the (T.D.) tensile axis orientations. Table 5 shows that, for different values of the critical Schmid factor M_c, associated with different strain levels, the number of grain boundary triple nodes where cavities would grow is significantly larger for (R.D.) than for (T.D.): this proves that the crystallographic texture is mainly responsible for the observed delayed cavitation for a (T.D.) tension with respect to the (R.D.) one.

An additional argument can be found in the possibility that twinning, which develops only when the tensile axis is parallel to (T.D.), could oppose the growth of cavities. An illustration of such an effect is given on Fig. 14 which shows the case of a cavity present at a triple node after a tensile test performed along (T.D.) up to fracture. The corresponding sample has been sectioned longitudinally and polished, so that no slip lines are visible. Nevertheless,

Table 5. Influence of the critical Schmid factor M_c value, considered as a decreasing function of the strain level, on the sign of the singularity parameter S, for 30 grain boundary triple points. The tensile test is assumed to be performed either along (R.D.) or along (T.D.)

M_c	(R.D.) Positive singularity	(T.D.) Positive singularity
0.40	11	1
0.38	15	6
0.34	16	9
0.30	20	11

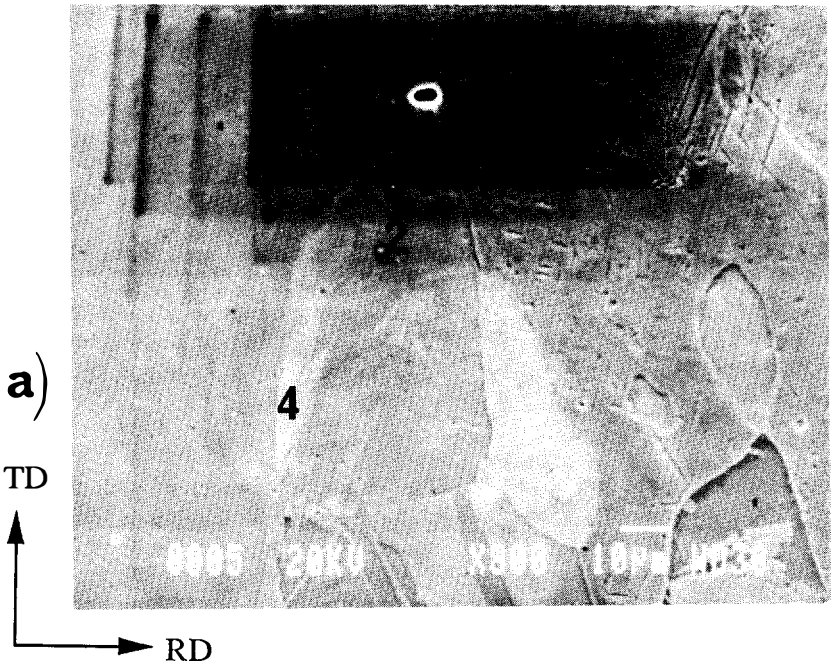

Grain I: Mk=**0.32**; **0.40**; 0.08
Grain II: Mk=0.23; **0.50**; **0.27**
Grain III: Mk=0.01; **0.44**; **0.43**
Grain IV: Mk=0.19; 0.16; 0.03

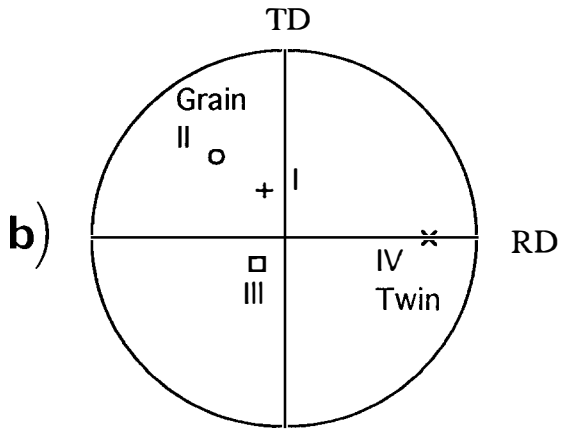

Fig. 14. (a) Cavity at a grain boundary triple node. The tensile test is performed along the transverse direction ($\epsilon = 25\%$). Observations on a sectioned sample. (b) [0002] pole figure for grains I, II, III and IV and Schmid factors for the prismatic slip systems in each grain.

the crystallographic orientation of each grain is identified. Grain II is unambiguously defined as a twinned area deriving from a grain orientation labelled as "grain IV", much more in agreement with the known crystallographic texture than grain II. Indeed, a detailed inspection of this sample area, both by S.E.M. and E.B.S.D., allows one to identify some remnants of the original grain IV. So, two S calculations are performed: the one for the initial triplet (I, IV, III) and the other for the transformed triplet (I, II, III). The corresponding S values are found to be $+38$ and $+15$, respectively. In both cases, the positive sign of S fits with the presence of a cavity but, in addition, the result suggests that twinning could slow down the cavitation process by making the intensity of the mean stress singularity decrease.

5. DISCUSSION

The proposed model is based upon some rough approximations and a number of assumptions. In our opinion, the most debatable points lie in the fact that grains are supposed to be uniformly deformed and that stresses are estimated within an elastic accommodation framework: in fact, more realistic hypotheses would have made the stress analysis of the great number of experimental situations under study and the comparison between numerical and experimental data almost untractable. Nevertheless, it can be stressed that we have used the results of the elastic analysis in a qualitative way, by considering only the sign (and partly the relative level) of the S parameter. Analogy with fracture mechanics and stress analysis at crack tips suggests that this is a reasonable way of doing things: in the actual plastically flowing tricrystals, stress singularities are surely smoothed over by plastic relaxation mechanisms; but there remains stress concentrations which are likely to be similar in sign and relative intensity to the elastic singularities.

Attention has been focused on triple nodes only and the influence of precipitate platelets on cavitation has been somewhat disregarded. Two main reasons may be put forward for that: firstly, precipitates play an obvious role in cavitation at large strain only, whereas we were mainly interested in the "formation" of cavities; secondly, though precipitates associated with grain boundary triple nodes surely induce *additional* stress concentrations, especially in the small grained material where they are rather frequent, it cannot be asserted that they induce cavitation in any case. In addition, since they are clearly not a necessary factor for cavitation in the coarse grained material, it can be concluded that incompatibility stress concentrations at triple nodes play the prominent role in the cavitation process. Consequently, the observed increase of the cavitation density with the decrease of the grain size can be simply understood as the result of the increase of the triple node density (while the precipitation state remains unchanged).

It could be argued that alphagenic elements may embrittle zirconium grain boundaries. Nevertheless, although our model obviously fails to take segregation phenomena into account, it would be hard to understand why such phenomena would be more active in the triple nodes associated with a positive mean stress singularity than in the others.

Acknowledgements—The material supply and the scientific and financial support of the C.E.A. (Commissariat à l'Energie Atomique, CEREM/SRMA, Saclay, France) are gratefully acknowledged.

REFERENCES

1. B. Legrand, *Phil. Mag. B* **49,** 171 (1984).
2. J. R. Donoso, A. T. Santhaman and R. E. Reed-Hill, *Proc. 2nd Int. Conf. on Mechanical Behavior of Materials* (ICM-2), Special Volume, pp. 515–537. ASM, Cleveland (1978).
3. P. Chemelle, D. B. Knorr, J. B. Van der Sande and R. M. Pelloux, *J. Nucl. Mater.* **113,** 58 (1983).
4. L. Allais, M. Bornert, T. Bretheau and D. Caldemaison, *Acta metall. mater.* **42,** 3865 (1994).
5. M. H. Yoo, *Metall. Trans. A* **12A,** 409 (1981).
6. J. L. Béchade, Rapport CEA-R-5659 (1994).
7. D. Watson, M. R. Warren and C. J. Beevers, *Can. Metall. Q.* **11,** 53 (1972).
8. J. Crépin and T. Bretheau, *Plasticity '95*, 17–21 July 1995. Sakai, Japan. Accepted.
9. F. Forscher, *Trans. AIME, J. Metals*, May, 536 (1956).
10. A. S. Argon, J. Im and R. Safoglu, *Metall. Trans. A* **6A,** 825 (1975).
11. W. Roberts, B. Lehtinen and K. E. Easterling, *Acta metall.* **24,** 745 (1976).
12. N. Laws and J. C. Lee, *J. Mech. Phys. Solids* **37,** 603 (1989).
13. F. Garofalo, *Fundamentals of Creep and Creep-Rupture in Metals*. The Macmillan Company, New York (1965).
14. J. Intrater and E. S. Machlin, *Acta metall.* **7,** 140 (1959).
15. C. Rey, P. Mussot, A. M. Vroux and A. Zaoui, *J. Physique*, Colloque C4, supplément au no. 4, Tome 46, C4-645-650 (1985).
16. G. Saada, *J. Phys. France* **50,** 2505 (1989).
17. A. Yu. Belov, *Phil. Mag. Lett.* **64,** 207–210 (1991).
18. E. S. Fisher and C. J. Renken, *Phys. Rev.* **135** (2A), 482 (1964).
19. E. Tenchkoff, ASTM-STP 966, 3 (1988).
20. S. Caré and T. Bretheau, *ICSMA 10* (edited by Oikawa *et al.*), Strength of materials, p. 891 (1994).

APPENDIX

Let $\mathbf{A}^{(i)}$ and $\mathbf{B}^{(i)}$ be respectively the unit vectors along the trace of the grain boundary (i) (Fig. A1), with the unit

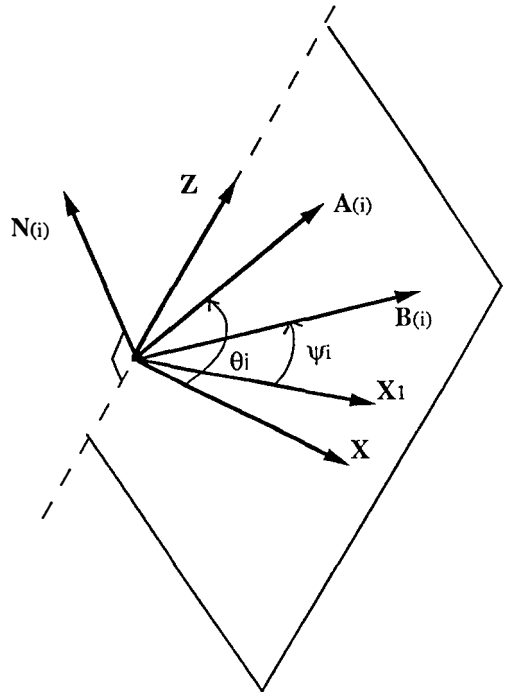

Fig. A1. Orientation of different traces of the grain boundary (i).

normal $\mathbf{N}^{(i)}$, in the plane $(\mathbf{X}, \mathbf{Y})$ normal to the junction line $\mathbf{Z}$ and in the plane $(\mathbf{X}_1, \mathbf{Y}_1)$ of the surface example. We write:

$$\mathbf{A}^{(i)} = \cos\theta_i \mathbf{X} + \sin\theta_i \mathbf{Y} \quad \mathbf{N}^{(i)} = \mathbf{A}^{(i)} \Lambda \mathbf{Z}. \tag{A1}$$

Let $\mathbf{P} = (P_{\alpha\beta})$ with $\alpha, \beta = 1\text{–}3$, the matrix defining the axes $(\mathbf{X}, \mathbf{Y}, \mathbf{Z})$ from $(\mathbf{X}_1, \mathbf{Y}_1, \mathbf{Z}_1)$.

We get:

$$\begin{aligned}\mathbf{N}^{(i)} &= \sin\theta_i \mathbf{X} - \cos\theta_i \mathbf{Y} = N_1 \mathbf{X}_1 + N_2 \mathbf{Y}_1 \\ &= \sin\theta_i (P_{11}\mathbf{X}_1 + P_{12}\mathbf{Y}_1 + P_{13}\mathbf{Z}_1) \\ &\quad - \cos\theta_i (P_{21}\mathbf{X}_1 + P_{22}\mathbf{Y}_1 + P_{23}\mathbf{Z}_1).\end{aligned} \tag{A2}$$

Since $\mathbf{B}^{(i)} = B_1 \mathbf{X}_1 + B_2 \mathbf{Y}_1$ is parallel to the vector $\mathbf{N}^{(i)} \Lambda \mathbf{Z}_1$, the angle Ψ_i between $\mathbf{X}_1$ and $\mathbf{B}^{(i)}$ is such that:

$$\tan\Psi_i = \frac{B_2}{B_1} = -\frac{N_1}{N_2}$$

$$= -\frac{P_{11}\sin\theta_i - P_{21}\cos\theta_i}{P_{12}\sin\theta_i - P_{22}\cos\theta_i}$$

$$= -\frac{P_{11}\tan\theta_i - P_{21}}{P_{12}\tan\theta_i - P_{22}}. \tag{A3}$$

Conversely, we get:

$$\tan\theta_i = \frac{P_{22}\tan\Psi_i + P_{21}}{P_{12}\tan\Psi_i + P_{11}}. \tag{A4}$$

Since the considered grain boundaries are actually half planes instead of planes, it must be checked that $\mathbf{A}^{(i)}$ and $\mathbf{B}^{(i)}$ belong to the same half-plane. The corresponding condition reads:

$$\cos(\mathbf{A}^{(i)} \Lambda \mathbf{Z}, \mathbf{B}^{(i)} \Lambda \mathbf{Z}) \geqslant 0, \tag{A5}$$

which allows an unambiguous determination of θ_i.